Small 16.29 (2020): 1907171

DOI: https://doi.org/10.1002/smll.201907171907171

WILEY-VCH

Instantaneous *in vivo* imaging of acute myocardial infarct by NIR-II luminescent nanodots

Sergio Mateos,[+] *José Lifante,*[+] *Chunyan Li, Erving C. Ximendes, Tamara Muñoz-Ortiz, Jingke Yao, María de la Fuente, Ángel Luis García Villalón, Miriam Granado, Irene Zabala Gutiérrez, Jorge Rubio Retama, Daniel Jaque,* Dirk H. Ortgies,* and Nuria Fernández*

M.Sc. S. Mateos, M.Sc. J. Lifante, M. de la Fuente, Prof. A. L. García Villalón, Prof. M. Granado, Prof. N. Fernández
Fluorescence Imaging Group, Departamento de Fisiología – Facultad de Medicina, Avda. Arzobispo Morcillo 2, Universidad Autónoma de Madrid, 28029 Madrid, Spain

Dr. E. C. Ximendes, M.Sc. T. Muñoz-Ortiz, M.Sc. J. Yao, Prof. D. Jaque, Dr. D. H. Ortgies
Fluorescence Imaging Group, Departamento de Física de Materiales – Facultad de Ciencias, Universidad Autónoma de Madrid, C/ Francisco Tomás y Valiente 7, 28049 Madrid, Spain
E-mail: daniel.jaque@uam.es
E-mail: dirk.ortgies@uam.es

C. Li
CAS Key Laboratory of Nano-Bio Interface, Suzhou Key Laboratory of Functional Molecular Imaging Technology, Division of Nanobiomedicine and i-Lab, Suzhou Institute of Nano-Tech and Nano-Bionics, Chinese Academy of Sciences, Suzhou 215123, China, University of Science and Technology of China, Hefei, 230036 China

I. Zabala Gutiérrez, Prof. J. Rubio Retama
Departamento de Química Física en Ciencias Farmacéuticas, Facultad de Farmacia, Plaza de Ramón y Cajal, s/n, Universidad Complutense de Madrid, 28040 Madrid, Spain

M.Sc. J. Lifante, Dr. Erving Ximendes, Prof. J. Rubio Retama, Prof. D. Jaque, Dr. D. H. Ortgies, Prof. N. Fernández
Nanobiology Group, Instituto Ramón y Cajal de Investigación Sanitaria, IRYCIS, Ctra. Colmenar km. 9.100, 28034 Madrid, Spain

[+] Both authors contributed equally to this work.

Keywords: near-infrared imaging, myocardial infarct, luminescence, nanoparticles, Ag_2S

Fast and precise localization of ischemic tissues in the myocardium after an acute infarct is being required by clinicians as the first step towards accurate and efficient treatment. Nowadays, diagnosis of a heart attack at early times is based on biochemical blood analysis (detection of cardiac enzymes) or by ultrasound-assisted imaging. Alternative approaches are investigated to overcome the limitations of these classical techniques (time-consuming procedures or low spatial resolution). As occurs in many other fields of biomedicine, cardiological preclinical imaging can also benefit from the fast development of nanotechnology. Indeed, bio-functionalized near-infrared-emitting nanoparticles are herein used for *in vivo* imaging of the heart after an acute myocardial infarct. Taking advantage of the superior acquisition speed of near-infrared fluorescence imaging, and of the efficient selective targeting of our near-infrared-emitting nanoparticles, *in vivo* images of the infarcted heart were obtained only a few minutes after the acute infarction event. This work opens the avenue towards cost-effective, fast and accurate *in vivo* imaging of the ischemic myocardium after an acute infarct.

1. Introduction

Cardiovascular diseases (CVDs) are responsible for the majority of deaths occurring in the world, especially in low-income and middle-income countries.[1] The increasing impact of CVDs makes it mandatory to improve the diagnostic capabilities of the medical community in order to enable cost-effective diagnosis of a cardiovascular event. In particular, fast diagnostic tools of CVDs need to be developed in order to achieve early diagnosis. The efficacy of recovery treatments increases substantially when the consequences of a cardiovascular event (such as an infarct) are known and treated in their early stages. Indeed, early diagnosis provides the extra time required to mitigate the consequences for the patient, avoiding to place large burdens on health systems.[2,3] Of particular relevance is the early diagnosis, assessment and treatment of an acute myocardial infarction (heart attack), where an occlusion event in the coronary arteries results in ischemia and lack of oxygen in the myocardium, often causing irreparable damage and/or death.[4] Currently, clinical methods to image and diagnose myocardial infarction rely on low resolution ultrasound imaging, relatively slow biochemical blood analysis, expensive and time-consuming instrumentation (MRI), as well as harmful and expensive nuclear medicine (X-Ray angiography, CAT).[5] The development of a new imaging technique capable of cost-effective, fast, and ionizing radiation-free visualization and diagnosis of the heart after an acute infarct remains an unaddressed challenge.[6]

Over the last decade advances made in the synthesis and modification of materials led to novel diagnostic techniques and therapies based on the use of nanoparticles as contrast agents.[7,8] For instance, imaging of infarcted hearts was recently demonstrated based on magnetic nanoparticles, liposomes and porous silicon (PSi) nanoparticles. [9–12] Despite the good results obtained by these systems, they are either not capable of *in vivo* imaging or require an expensive apparatus (such as MRI). These limitations can be overcome by employing luminescent nanoparticles (LNPs). LNPs were, indeed, used for imaging of the infarcted heart (see **Table 1**).[13,14] Unfortunately, the intrinsic limitations of sub-800 nm

fluorescence imaging (such as poor penetration depth and undesirable overlap with autofluorescence) reduces the potential application of these nanoparticles at the clinical level. Furthermore, as can be observed from **Table 1,** *in vivo* imaging of the infarcted heart by employing these LNPs was only obtained hours/days after the infarct. The application of luminescent nanoparticles for *in vivo* fast (minutes) diagnosis of infarcted hearts after an acute event is still a pending task.

The limitations of sub-800 nm fluorescence imaging can be overcome by the use of LNPs emitting in the second near infrared window (NIR-II).[15–17] The NIR-II extends from 1000 up to 1700 nm and it is a spectral range where tissues become partially transparent as their extinction coefficient minimizes.[18,19] In addition, NIR-II fluorescence imaging simultaneous reduces the autofluorescence background and the tissue-induced scattering,[20,21] thereby enabling better performance than sub-800 nm emitting NPs like the examples in **Table 1**. The development of LNPs operating in the NIR-II made *in vivo* whole-body imaging in small animals with outstanding resolutions and signal-to-background ratios possible. NIR-II *in vivo* fluorescence imaging has been demonstrated by using rare-earth-doped NPs,[22–25] carbon-based NPs,[26–28] semiconducting organic polymers and NPs,[29–32] or semiconductor quantum dots (QDs).[33–35] In the latter group Ag_2S nanodots (NDs) have become quite popular due to their facile synthesis, good brightness, and improved biocompatibility in comparison with other QDs containing more toxic elements such as Cd or Pb.[36–38] Ag_2S NDs have been successfully employed for *in vivo* imaging of cancer,[39,40] vessel imaging and biodistribution studies,[41–44] photothermal treatments,[45–47] contactless thermal sensing,[48] theragnostics,[47,49,50] and imaging of the cardiovascular system.[51,52] Some of these applications are based on the appropriate surface decoration of Ag_2S NDs that give them affinity to the targeted tissues such as tumors. Selective targeting of ischemic myocardial tissues is also possible based upon the fact that during a myocardial event the angiotensin receptor 1 (AT1R) of the angiotensin-renin system is overexpressed in the myocardium.[53]

The natural ligand for the AT1R is angiotensin II (AngII), which has demonstrated to keep its high binding efficacy also when conjugated to nanoparticles.[54] Dvir et al. explored this functionalization for imaging of damaged myocardium tissues in mice by employing nano-size PEGylated liposomes conjugated with AngII and loaded with an organic dye (DyLight649). The authors obtained *ex vivo* fluorescence images of infarcted hearts 24 hours after the infarct.[55] Very recently, AngII-biofunctionalized Ag_2S NDs were also successfully employed for NIR-II fluorescence imaging of myocardial infarction in an *ex vivo* Langendorff model,[56] evidencing the potential of the AngII functionalization for fast imaging of a heart attack. But the application of AngII-biofunctionalized Ag_2S NDs for direct NIR-II *in vivo* heart imaging is still left to be demonstrated. Efficient targeting of AngII-biofunctionalized Ag_2S NDs at the *ex vivo* level does not automatically ensure their suitability for *in vivo* applications. When dealing with *in vivo* experiments with systemic intravenous injection, the targeting capability of AngII-biofunctionalized Ag_2S NDs can be affected by the formation of a protein corona.[57–60] Also, efficient accumulation at the infarcted myocardial tissues requires minimum retention or clearance of AngII-biofunctionalized Ag_2S NDs by other organs, such as the liver and kidneys.

In this work we have employed AngII-functionalized Ag_2S NDs for NIR-II *in vivo* imaging of the heart at short times (minutes) after a myocardial infarct. The analysis of time-course experiments allowed to evaluate the speed of selective accumulation of AngII-functionalized Ag_2S NDs at ischemic myocardial tissues after their intravenous injection. A comparison between the biodistribution patterns obtained with the AngII and PEG-functionalized Ag_2S NDs was employed to evaluate the selectivity of our approach.

2. Results and Discussion

Figure 1a illustrates schematically the approach followed in this work. Shortly, a myocardial infarction was induced in a mouse by ligating its left descending coronary artery (LAD) for 30

minutes followed by 30 minutes reperfusion (for details see **Experimental Section**). This leads to a significant overexpression of the AT1R receptor in the affected myocardial tissue (schematically in **Figure 1a**),[53,55] Directly after reperfusion, AngII-functionalized Ag_2S NDs where intravenously injected (100 μl, 1.5 mg mL^{-1}, retroorbital). **Figure 1b** shows the Transmission Electron Microscopy (TEM) micrograph of the the AngII-functionalized Ag_2S NDs. Binding of the AngII-functionalized Ag_2S NDs to the damaged myocardium tissue was monitored through their NIR-II luminescence centered at 1200 nm (see **Figure 1c**), when illuminated by an 808 nm diode laser at relatively low power densities (0.2 W cm^{-2}) and the fluorescence generated by Ag_2S NDs was collected and recorded by an InGaAs infrared camera. As we were interested in the fast diagnosis of the infarcted heart, fluorescence images were obtained every 5 minutes during the first hour after intravenous injection of the NIR-II probes. For non-targeting control experiments PEGylated Ag_2S nanoparticles (for their TEM see **Figure S1** in the Supporting Information) were employed. Despite the different surface decorations, these two nanoparticles showed very similar hydrodynamic radii, close to 10 nm (see **Figures 1d** and **e**). The two different functionalizations do not produce any relevant change in the emission spectra of the particles, as demonstrated in the literature.[56]

Figure 2a shows the optical, NIR-II fluorescence and merged *in vivo* images of mice as obtained 10 minutes after the intravenous injection of Ag_2S NDs (40 minutes after the infarct induction). The complete series of NIR-II images taken during the whole experiment (30 s to 60 minutes) are included in the Supporting Information as **Figure S3**. The NIR-II fluorescence images obtained after performing the heart surgery and injection of Ag_2S-AngII nanoparticles (top row), after surgery and injection of non-targeting PEG-decorated Ag_2S (middle row) and at the bottom after a sham surgery (no infarct) and injection of targeted Ag_2S-AngII nanoparticles are included. The first row reveals a preferential accumulation of Ag_2S-AngII NDs at the infarcted heart. On the contrary, in absence of an infarct or when using PEGylated Ag_2S NDs, NIR-II fluorescence images clearly demonstrate preferential

accumulation in the abdomen due to the retention of nanoparticles in the liver. The NIR-II fluorescence images included in **Figure 2a** demonstrated the successful *in vivo* targeting capability of the employed functionalized Ag_2S-AngII NDs and their preferential adhesion to acutely damaged myocardium tissues. Note that after intravenous injection Ag_2S nanoparticles were only preferentially accumulated at the damaged myocardium tissues, when AngII was present as their surface ligand. The two control experiments showed that without targeting or without a myocardial infarct no accumulation in the heart takes place.

In order to evaluate the speed of such preferential targeting of the damaged myocardium, time-course experiments were performed. **Figure 2b** shows the average time evolution of the NIR-II fluorescence generated at the heart and liver after intravenous injection of Ag_2S-AngII NDs in three mice subjected to an induced infarct (See **Figure S4** for individual time courses). Data included in **Figure 2b** reveals that the AngII-functionalized nanoparticles accumulate quickly at the infarcted heart. Indeed, accumulation is mainly produced during the first 10 minutes following intravenous injection. **Figure 2b** also includes the time evolution of the NIR-II fluorescence signal generated by the Ag_2S NDs accumulated in the liver. Note that, contrary to what is observed at the heart, the NIR-II fluorescence signal generated from the liver decreases monotonously with time, indicating an initial retention by the liver likely followed by a gradual release. **Figure 2c** shows the time evolution of the NIR-II fluorescence intensity generated by PEGylated Ag_2S NDs accumulated at both the heart and liver after intravenous injection in three mice subjected to an acute infarct (See **Figure S5** for individual time courses). In this case, the time evolution of the NIR-II intensity generated at both organs follows a completely different pattern. Preferential retention at the liver is observed, even for very short times. Note that after intravenous injection, the NIR-II intensity generated at the liver remains virtually constant indicating a long-term retention of PEGylated Ag_2S NDs at the liver. At the same time, no significant preferential accumulation at the heart is observed. At short times after injection, PEGylated Ag_2S NDs are present at the heart, due to their

permanence in the circulatory system. Nevertheless, the NIR-II fluorescence generated by the PEGylated Ag_2S NDs at the heart decreases monotonously with time. Finally, **Figure 2d** illustrates the time course for a sham surgery (no infarct+Ang II). The Ag_2S-AngII NDs accumulate at the liver and the signal is decreasing over the time-course, while the minimal signal observed at the heart shortly after injection is also decreasing rapidly. This indicates good clearance of Ag_2S-AngII, when no myocardial infarction has occurred. The time profiles included in **Figures 2b, c** and ~~c~~ **d** do not only reveal the suitability of AngII-decorated Ag_2S NDs for selective targeting of the damaged myocardium after the acute heart attack, but also reveal their capability for fast diagnosis as selective accumulation is produced on a short time scale: 10 minutes after the injection are sufficient time to observe a clear and specific signal from ischemic myocardial tissues.

Con formato: Fuente: Negrita

The characteristic circulation time of AngII-functionalized Ag_2S NDs was estimated by means of an experiment in which the time evolution of the luminescence intensity generated at the femoral artery was recorded after intravenous injection of Ag_2S NDs into both, an ischemic and a sham-operated mouse (see **Section S6** of **Supporting Information)**. In both cases, the NIR-II fluorescence generated by the AngII-functionalized Ag_2S NDs circulating in the bloodstream was characterized by an initial increment that lasted approximately 2 minutes and that is associated to the time required for full incorporation of the injected NDs into the blood stream. For times longer than 2 minutes a monotonous decrease of intensity is observed in both cases. This, in turn, reflects the limited circulation time of the injected NDs independently on whether or not there is damage at the myocardium. The estimation of the decay time provided 500 s in both cases. Hence, we conclude that independently of the presence or absence of damage at the myocardium, the AngII-functionalized Ag_2S NDs possess a circulation time of approximately 20 minutes.

In order to further corroborate that the *in vivo* NIR-II fluorescence signal detected from the myocardium in **Figure 2a** is unequivocally correlated with the presence of Ag_2S NDs, the

animals were sacrificed one hour after the NPs injection. The hearts were immediately dissected and analyzed via NIR-II hyperspectral imaging. A detailed description of the experimental system used for NIR-II hyperspectral imaging can be found in the **Experimental Section**. **Figure 3a** shows luminescence images obtained at 1000, 1200 and 1500 nm of explanted hearts corresponding to the three situations studied in this work. The top row illustrates the case of an infarcted heart after intravenous injection of Ag_2S-AngII NDs (Infarcted+Ag_2S-AngII case). No luminescence neither at 1000 nor at 1500 nm was observed. The fluorescence image obtained at 1200 nm shows a clear signal generated at the top of the heart, where the most relevant damage of myocardial tissue has been produced. The fact that the fluorescence image is detected at 1200 nm suggest that the luminescence contrast is being provided by the Ag_2S-AngII NDs. The emission spectra obtained from the analysis of the hyperspectral cube as obtained in the top area of the heart are included in **Figure 3b** (more spectra can be found in **Figure S7**). It well matches the emission spectra of Ag_2S NDs in a colloidal suspension (see **Figure 1c**), clearly indicating that the observed luminescence can be attributed to the selective attachment of Ag_2S-AngII NDs to the ischemic myocardium. The middle row in **Figure 3a** shows the fluorescence images at the three analyzed wavelengths of an infarcted heart after intravenous injection of PEGylated Ag_2S NDs (Infarcted+Ag_2S-PEG case). In this case, only a very weak signal is observed at 1200 nm. This suggests a minimal accumulation of NDs. Data included in **Figure 3b** reveals that the emission spectrum obtained in this case is broadband centered at 1200 nm although weaker than for AngII-Ag_2S NDs. This can be correlated with a small presence of PEGylated Ag_2S NDs in the ischemic myocardium tissues probably due to the enhanced permeability and retention effect (EPR), which can occur in ischemic myocardial tissues.[49,53] Finally, the bottom row in **Figure 3a** shows the NIR-II luminescence images obtained from a healthy heart after intravenous injection of AngII Ag_2S NDs (Sham+Ag_2S-AngII case). Again, no signal is observed at 1000 and 1500 nm and the fluorescence image obtained at 1200 nm is barely above the

background. The emission spectra obtained for this healthy control heart is also included in **Figure 3b**. The obtained spectrum does not resemble the emission spectrum of Ag_2S NDs, indicating negligible accumulation in the healthy heart and the necessity of an ischemic event in order to increase AT1R expression and accumulation.

Triphenyl tetrazolium chloride (TTC) staining further corroborated these findings as shown in **Figure S8** in the Supporting Information, confirming that a control heart (sham operation) did not show damages and was in fact a healthy heart (**Figure S8a**) while an infarcted heart with damaged tissue principally in the tip, which had been exposed to Ag_2S-AngII NDs, is shown in **Figure S8b**. A collateral question rising at this point is the origin of the fluorescence observed in the spectra in **Figure 3** (likely autofluorescence) generated by the heart in absence of Ag_2S NDs. This question is out of the scope of this work and will deserve detailed investigation. Nevertheless, we state at this point that this emission band very likely corresponds to the NIR-II autofluorescence of heart.

In order to further analyze the presence of an infarct and the overexpression of AT1R, a reverse transcriptase qualitative polymerase chain reaction (qt-PCR) was performed with samples obtained from infarcted hearts. **Figure 3c** shows the percentage of AT1R expression as obtained for healthy hearts (sham) and infarcted hearts based on the mRNA expression levels that were analyzed as described in the **Experimental Section**. As expected, the shams present a low expression of AT1R, whereas it is significantly elevated in the damaged myocardial tissues. The data included in **Figure 3c** can be correlated with the integrated intensity of the emission spectra included in **Figure 3b** and is presented in **Figure 3d**. This graph effectively visualizes the targeting efficiency of our AngII-functionalized Ag_2S NDs for the detection of ischemic myocardium. It also allows to quantify it. Note that the infarct induction leads to a relative increment in the AT1R expression of less than 50% in **Figure 3c** whereas the NIR-II fluorescence signal associated with the selective accumulation of Ag_2S-

AngII NDs shows a 10-fold increment. This, again, reveals a highly efficient targeting at short circulation times.

Finally, the AT1R-targeting capabilities of our AngII-functionalized Ag_2S NDs were further investigated by the evaluation of biodistribution patterns. The NIR-II luminescence images of exerted organs from the three cases studied in **Figure 3** were systematically acquired. **Figure 4a** shows that PEGylated Ag_2S NDs accumulate preferentially in the liver and spleen, while all other organs did not ~~show any~~sufficient infrared luminescence on this scale, as was the case for the control experiment without an infarct, which also resulted in accumulation in liver and spleen. In contrast, in the organs from the mouse injected with AngII-functionalized Ag_2S NDs after the infarct induction, luminescence is only ~~present~~ visible in the heart and in the lungs. In this case, no ~~significant~~ substantial retention of AngII-functionalized Ag_2S NDs by either liver or spleen has been observed, in good agreement with the data included in **Figure 2b**. Nevertheless, an individual quantification of the residual luminescence in each organ revealed residual luminescence signal and therefore the presence of NDs as demonstrated in the two histograms (**Figure 4b** and **c**). **Figure 4b** represents the PEG control and shows apart from the clear accumulation in liver and spleen, a minimal signal in stomach and liver. **Figure 4c** demonstrates that in addition to the clearly visible signal in the heart and lungs for the case of the infarct with AngII-functionalized NDs, there is also some non-trivial signal in the liver, stomach, spleen and intestine. These residual signals in both cases, together with the generally in the literature observed tendency for Ag_2S nanoparticles,[REFs] indicate a preferential clearance of the PEGylated and the AngII-functionalized NDs via the biliary pathway and excretion through the feces. The accumulation at the lungs of the AngII-functionalized Ag_2S NDs was initially surprising but it could be explained due to a dysfunction of the alveolar-capillary barrier that may lead to pulmonary congestion,[61,62] which would cause the extravasation of the non-targeted NPs.[63] Moreover, mechanical ventilation may cause ventilator-induced lung injury (VILI) even when the least injurious ventilator settings are

Con formato: Fuente: Negrita
Con formato: Fuente: Negrita
Con formato: Fuente: Negrita
Con formato: Fuente: Negrita
Con formato: Subíndice

used.[64] In the pathogenesis of VILI inflammation plays an important role, and upregulation of lung angiotensin receptors could be present as part of inflammatory response.[65]

3. Conclusion

This work demonstrates that fast and highly selective *in vivo* heart imaging after an acute infarct is, indeed, possible by using NIR-II emitting Ag_2S NDs functionalized with the peptide angiotensin II. Results included in this work demonstrate how the overexpression of the AT1R receptor after an acute infarct enables the instantaneous (< 10 minutes) and selective targeting of intravenously injected AngII-functionalized Ag_2S NDs to ischemic myocardial tissues. The strong luminescence of Ag_2S NDs in the second infrared transparency window makes real time *in vivo* visualization of hearts damaged by an acute infarct possible at the earliest time. Comparison of the hyperspectral images of *ex vivo* organs were employed to reinforce the high specificity of AngII-functionalized Ag_2S nanoNDs for attaching to ischemic myocardial tissues even during systemic injection.

This work introduces to the scientific community NIR-II emitting nanoparticles for fast *in vivo* imaging and diagnosis of the heart after an acute infarct in a small animal model. It constitutes a first step towards early and speedy diagnosis at the pre-clinical level of myocardial infarct and, therefore, could contribute to the development of new therapy routes. In addition, the high targeting ability of AngII-functionalized Ag_2S NDs for the detection and localization of ischemic myocardial tissues also opens the door to new therapy approaches based on drug delivery or for taking advantage of the ability of Ag_2S NDs to produce simultaneous local hyperthermia and contactless thermal sensing.

4. Experimental Section

Ag_2S NDs: Ag_2S-AngII were obtained from SINANO Int (China) at a concentration of 1.5 mg mL^{-1} in PBS. Ag_2S-AngII are coated with polyethyleneglycol and further modified via the carboxy terminus of the PEG with angiotensin II and 4 Glycine residues as spacer (Gly-Gly-

Gly-Gly-Asp-Arg-Val-Tyr-Ile-His-Pro-Phe). The Ag_2S-PEG non-targeted nanoparticles were synthesized and characterized as given in previous publications.[38] Shortly, silver diethyldithiocarbamate AgDDTC (0.1 mmol) was dispersed in dodecanethiol (5 mL). The mixture was submitted to vacuum for 10 minutes to remove air and then filled with N_2. After that, the mixture was heated to 190 ºC with a heating rate of 20 ºC min^{-1} and under slow magnetic stirring. The temperature was kept for 1 hour and later cooled down to room temperature naturally. The synthesized nanoparticles were collected by addition of absolute ethanol (10 mL), reducing the colloidal stability of the LNPs for collection via centrifugation (10,000 rpm for 10 minutes). This process was repeated twice. The as-prepared product was re-dispersed in chloroform (10 mL) and stored for further steps. With the aim of providing hydrophilicity to the synthesized LNPs, they were treated with 11-mercaptoundecanoic acid (MUA). This molecule introduced carboxylic groups on the surface of the nanoparticles, which provided colloidal stability in water. With that purpose, MUA (20 mg, 0.1 mmol) of MUA was added to a dispersion of Ag_2S nanoparticles in chloroform (1 mL, 1 mg mL^{-1}). After that, the mixture was sonicated in an ultrasonic bath for 10 minutes until the Ag_2S nanoparticles lost their colloidal stability and precipitated in the bottom of the flask. The precipitate was collected and dispersed in PBS (1 mL) at pH 7.4. The resulting nanoparticles exhibit a Z-potential of –34 mV due to the presence the negatively charged carboxylate groups on the surface of the nanoparticles. Subsequently these nanoparticles were covered with PEG (Mw=2500 g/mol) via EDC/NHS coupling. EDC (0.5 mg) and sulfo-NHS (0.7 mg) were dissolved in PBS (1 mL) containing the previously prepared Ag_2S NDs (1 mg) and mPEG-NH_2 (1 mg). The mixture was gently stirred for 2 hours and after this time the nanoparticles were collected by centrifugation at 12.000 rpm for 4 hours. This process was repeated three times and the resulting nanoparticles were dispersed in PBS (1 mL) and stored at 4 ºC. The Z-potential of these nanoparticles is reduced to –17 mV, as a result of the transformation of part of the carboxylate groups into amide bonds.

Morphological characterization: Transmission electron microscopy was performed on a JEOL JEM 1010 microscope operating at 80 kV. The carbon coated copper TEM grid was loaded with sample by placing one drop of a dilute aqueous dispersion onto it and letting it dry for 10 minutes. The size distributions were obtained through analysis via ImageJ of ensembles of over 200 particles in randomly selected areas of the enlarged micrographs. *Animal Studies*: 17 CD1 2-month-old male and female mice were employed in this study. All animal experiments were approved by the Animal Ethics Committee of the Universidad Autónoma de Madrid and conducted in accordance with the European Union directive 63/2010UE and the Spanish regulation RD 53/2013. The acute myocardial ischemia-reperfusion injury was performed through ligation of the Left Anterior Descending Artery (LAD) following the protocol described by Xu et al.[66] Sedation of the animal was achieved through a combination of Xylazine (0.2 mL) and Ketamine (0.3 mL) mixed with saline solution (0.15 mL) and administrating 0.15 ml of anesthetic per 30 g of animal body weight, via intraperitoneal injection. Prior to the intervention, the chest and the left side of the intercostal area of the animal were shaved and cleaned with 95% alcohol. Afterwards, orotracheal intubation was performed. For the orotracheal intubation of the animal, we exposed the trachea by a median cervical skin incision with the animal in a supine position and separated the lobes of the thyroidal gland and the muscle below, exposing the trachea. This allowed the introduction of an intubation tube (Insyte-W, 0.9 x 25 mm) with the help of a needle, which had the tip cut to prevent damage, confirming the correct position inside the trachea with a magnifying glass. After a correct orotracheal intubation, a constant flow of 0.8% isoflurane anesthetic in 100% oxygen with a flow rate of 170 breaths/minute and an external positive end-expiratory airway pressure (PEEP) from 2 - 10 cmH_2O was maintained by an external small animal ventilator (VentElite 55-7040, Harvard Apparatus). To maintain the temperature of the animal, the procedure was performed on a heating pad and the animal temperature was controlled with a rectal probe. In order to gain access to the heart, the

intercostal space between the 3rd and 4th ribs was opened, the pericardium was removed and the LAD was identified below the left auricle. The ligation was performed before the bifurcation of the LAD with an 8-0 silk suture. Between the LAD and silk suture, before closing the knot, a plastic tube of 2-3 mm was placed in order to be able to reperfusion. The ligation of the LAD was performed for 30 minutes until reperfusion, which was maintained for another 30 minutes. Finally, the animals were moved to the imaging setup where they were retroorbitally injected with specific NDs always with 100 µl of a solution with a concentration of 1.5 mg mL^{-1}.

Quantification of AT-1 gene expression in myocardial tissue by RT-qPCR: Total RNA was extracted from 100 mg of myocardial tissue using the Trizol method and quantified with a Nanodrop2000 spectrometer (Thermo Fisher Scientific, Hampton, NH, EE.UU).[67] Afterwards, 1 µg of total RNA was retrotranscribed into cDNA using a high capacity cDNA reverse transcription kit (Applied Biosystems, Foster City, CA, USA). The mRNA levels of AT-1 were measured by quantitative real-rime PCR. The assay was performed by using an on-demand assay probe (Applied Biosystems, Foster City, CA, USA) for this specific gene (Mm_ 00616371_m1). TaqMan Universal PCR Master Mix (Applied Biosystems, Foster City, CA, USA) was used for amplification in a Step One thermocycler (Applied Biosystems, Foster City, CA, USA). To determine relative expression levels the ΔCT method was used.[68] Values were normalized to the housekeeping gene 18S. Data are represented by the mean ± SEM and analyzed by unpaired t-student (n = 3 samples/experimental group). Differences were considered statistically significant when $p < 0.05$.

Infrared fluorescence Imaging: The anesthetized and operated animals were located in the field of view of an InGaAs camera (Xeva1.7-320) with high sensitivity in the IR spectral range (1000 – 1700 nm). Excitation was performed by a fiber-coupled 808 nm laser diode (LIMO) placed next to the camera objective in order to create a spot of 35 cm^2, resulting in an illumination of 0.2 W/cm^2. The 808 nm scattering background of the laser diode was

eliminated by 2 long pass filter with a cutoff wavelength of 850 nm (Thorlabs FEL850) and 1050 nm (Thorlabs FEL1050) between the objective and the camera. All 3 cases studied imaged in this work (Infarct+AngII, Infarct+PEG, and No Infarct+AngII) were performed with groups of 3 mice each (n = 3). The standard error represented throughout this work is given as the standard error of the mean (SEM).

Hyperspectral Imaging: The freshly dissected hearts were excited with the same continuous laser (LIMO) via a fiber of 808 placed next to the camera objective and power and distance were regulated to achieve an illumination intensity of 50 mW/cm^2. An exposure time of 20 s and a spectral resolution of 10 nm was selected for all hyperspectral imaging studies. A short-pass filter (Thorlabs FES0850) was placed immediately in front of the laser fiber to minimize specular and diffuse reflection effects. The scattered light emitted from the sample was transmitted through two consecutive long-pass filter (Thorlabs FL0850) that were intended to suppress signal from the laser. Tube and shortwave infrared (SWIR) lenses were used as a relay to build up the fluorescence image on a Bragg tunable filter which allows to select a specific wavelength of the incoming light. A second tube lens focuses after the filtered light on an infrared camera (ZephIRTM 1.7) to produce a monochromatic image, while the non-filtered light follows a different optical path. To cover a specific spectral range, each monochromatic image needed to be acquired and then stored on a computer while the angle of the BTF rotation stage is set to the next wavelength. After n steps, one would then have what is called a HSI cube, i.e. a 3D spatial map of spectral variation: the first two dimensions providing spatial information and a third dimension accounting for the spectral information. The intensity values of a particular pixel in a HIS cube characterize its unique spectral fingerprint.[69]

Spectroscopic Characterization: The emission spectra were obtained upon excitation with a fiber-coupled 790 nm laser diode (Lumics) focused in a quartz cuvette filled with the aqueous dispersion of Ag_2S NDs (concentration 1.5 mg mL^{-1}). The luminescence signal was collected

by an InGaAs camera (Andor iDus DU490A) after passing through appropriate filters and being spectrally analyzed by an Andor Shamrock 193i spectrometer.

Supporting Information
Supporting Information providing additional characterization data (TEM, FTIR, staining) and more detailed NIR-II imaging (time courses, ex vivo) is available from the Wiley Online Library or from the author.

Acknowledgements
Support by the Ministerio de Economía y Competitividad de España (MAT2016-75362-C3-1-R) and (MAT2017-83111R), by the Instituto de Salud Carlos III (PI16/00812), by the Comunidad Autónoma de Madrid (B2017/BMD-3867RENIMCM), co-financed by the European Structural and investment funds, is acknowledged. Additionally, the investigation was supported by the European Commission Horizon 2020 project NanoTBTech, the Fundación para la Investigación Biomédica del Hospital Universitario Ramón y Cajal project IMP18_38 (2018/0265), and also by COST action CM1403. D. H. O. is grateful to the Instituto de Salud Carlos III for a Sara Borrell scholarship (No. CD17/00210). The authors are grateful to David Sabador Osuna for preparing Figure 1a.

Received: ((will be filled in by the editorial staff))
Revised: ((will be filled in by the editorial staff))
Published online: ((will be filled in by the editorial staff))

References

[1] S. Kaptoge, L. Pennells, D. De Bacquer, M. T. Cooney, M. Kavousi, G. Stevens, L. M. Riley, S. Savin, T. Khan, S. Altay, P. Amouyel, G. Assmann, S. Bell, Y. Ben-Shlomo, L. Berkman, J. W. Beulens, C. Björkelund, M. Blaha, D. G. Blazer, T. Bolton, R. Bonita Beaglehole, H. Brenner, E. J. Brunner, E. Casiglia, P. Chamnan, Y.-H. Choi, R. Chowdry, S. Coady, C. J. Crespo, M. Cushman, G. R. Dagenais, R. B. D'Agostino Sr, M. Daimon, K. W. Davidson, G. Engström, I. Ford, J. Gallacher, R. T. Gansevoort, T. A. Gaziano, S. Giampaoli, G. Grandits, S. Grimsgaard, D. E. Grobbee, V. Gudnason, Q. Guo, H. Tolonen, S. Humphries, H. Iso, J. W. Jukema, J. Kauhanen, A. P. Kengne, D. Khalili, W. Koenig, D. Kromhout, H. Krumholz, T. Lam, G. Laughlin, A. Marín Ibañez, T. W. Meade, K. G. M. Moons, P. J. Nietert, T. Ninomiya, B. G. Nordestgaard, C. O'Donnell, L. Palmieri, A. Patel, P. Perel, J. F. Price, R. Providencia, P. M. Ridker, B. Rodriguez, A. Rosengren, R. Roussel, M. Sakurai, V. Salomaa, S. Sato, B. Schöttker, N. Shara, J. E. Shaw, H.-C. Shin, L. A. Simons, E. Sofianopoulou, J. Sundström, H. Völzke, R. B. Wallace, N. J. Wareham, P. Willeit, D. Wood, A. Wood, D. Zhao, M. Woodward, G. Danaei, G. Roth, S. Mendis, O. Onuma, C. Varghese, M. Ezzati, I. Graham, R. Jackson, J. Danesh, E. Di Angelantonio, *Lancet Glob. Heal.* **2019**, *7*, e1332.

[2] M. Mahmoudi, M. Yu, V. Serpooshan, J. C. Wu, R. Langer, R. T. Lee, J. M. Karp, O. C. Farokhzad, *Nat. Nanotechnol.* **2017**, *12*, 845.

[3] F. Sanchis-Gomar, C. Perez-Quilis, R. Leischik, A. Lucia, *Ann. Transl. Med.* **2016**, *4*, 1.

[4] E. Ruvinov, T. Dvir, J. Leor, S. Cohen, *Expert Rev. Cardiovasc. Ther.* **2008**, *6*, 669.

[5] F. A. Flachskampf, M. Schmid, C. Rost, S. Achenbach, A. N. DeMaria, W. G. Daniel, *Eur. Heart J.* **2011**, *32*, 272.

[6] C. M. Kramer, A. J. Sinusas, D. E. Sosnovik, B. A. French, F. M. Bengel, *J. Nucl.*

Med. **2010**, *51*, 107S.

[7] O. Lozano, A. Torres-Quintanilla, G. García-Rivas, *J. Control. Release* **2018**, *271*, 149.

[8] J. Bejarano, M. Navarro-Marquez, F. Morales-Zavala, J. O. Morales, I. Garcia-Carvajal, E. Araya-Fuentes, Y. Flores, H. E. Verdejo, P. F. Castro, S. Lavandero, M. J. Kogan, *Theranostics* **2018**, *8*, 4710.

[9] D. E. Sosnovik, E. A. Schellenberger, M. Nahrendorf, M. S. Novikov, T. Matsui, G. Dai, F. Reynolds, L. Grazette, A. Rosenzweig, R. Weissleder, L. Josephson, *Magn. Reson. Med.* **2005**, *54*, 718.

[10] D. E. Sosnovik, E. Garanger, E. Aikawa, M. Nahrendorf, L. Jose-Figuiredo, G. Dai, F. Reynolds, A. Rosenzweig, R. Weissleder, L. Josephson, *Circ. Cardiovasc. Imaging* **2009**, *2*, 460.

[11] M. J. Lipinski, M. T. Albelda, J. C. Frias, S. A. Anderson, D. Luger, P. C. Westman, R. O. Escarcega, D. G. Hellinga, R. Waksman, A. E. Arai, S. E. Epstein, *Cardiovasc. Revascularization Med.* **2016**, *17*, 106.

[12] M. P. A. Ferreira, S. Ranjan, S. Kinnunen, A. Correia, V. Talman, E. Mäkilä, B. Barrios-Lopez, M. Kemell, V. Balasubramanian, J. Salonen, J. Hirvonen, H. Ruskoaho, A. J. Airaksinen, H. A. Santos, *Small* **2017**, *13*, 1.

[13] D. E. Sosnovik, M. Nahrendorf, N. Deliolanis, M. Novikov, E. Aikawa, L. Josephson, A. Rosenzweig, R. Weissleder, V. Ntziachristos, *Circulation* **2007**, *115*, 1384.

[14] M. Nahrendorf, D. E. Sosnovik, P. Waterman, F. K. Swirski, A. N. Pande, E. Aikawa, J. L. Figueiredo, M. J. Pittet, R. Weissleder, *Circ. Res.* **2007**, *100*, 1218.

[15] G. Hong, A. L. Antaris, H. Dai, *Nat. Biomed. Eng.* **2017**, *1*, 0010.

[16] J. Hu, D. H. Ortgies, E. Martín Rodríguez, F. Rivero, R. Aguilar Torres, F. Alfonso, N. Fernández, G. Carreño-Tarragona, L. Monge, F. Sanz-Rodriguez, M. del C. Iglesias, M. Granado, A. L. García-Villalon, J. García Solé, D. Jaque, *Adv. Opt. Mater.* **2018**, *6*, 1800626.

[17] D. Jaque, C. Richard, B. Viana, K. Soga, X. Liu, J. García Solé, *Adv. Opt. Photonics* **2016**, *8*, 1.

[18] A. M. Smith, M. C. Mancini, S. Nie, *Nat. Nanotechnol.* **2009**, *4*, 710.

[19] E. Hemmer, A. Benayas, F. Légaré, F. Vetrone, *Nanoscale Horizons* **2016**, *1*, 168.

[20] B. del Rosal, I. Villa, D. Jaque, F. Sanz-Rodríguez, *J. Biophotonics* **2016**, *9*, 1059.

[21] B. del Rosal, A. Benayas, *Small Methods* **2018**, *2*, 1800075.

[22] L. Labrador-Páez, E. C. Ximendes, P. Rodríguez-Sevilla, D. H. Ortgies, U. Rocha, C. Jacinto, E. Martín Rodríguez, P. Haro-González, D. Jaque, *Nanoscale* **2018**, *10*, 12935.

[23] Y. Liu, D. Tu, H. Zhu, X. Chen, *Chem. Soc. Rev.* **2013**, *42*, 6924.

[24] B. Liu, C. Li, P. Yang, Z. Hou, J. Lin, *Adv. Mater.* **2017**, *29*, 1605434.

[25] I. Villa, A. Vedda, I. X. Cantarelli, M. Pedroni, F. Piccinelli, M. Bettinelli, A. Speghini, M. Quintanilla, F. Vetrone, U. Rocha, C. Jacinto, E. Carrasco, F. S. Rodríguez, Á. Juarranz, B. del Rosal, D. H. Ortgies, P. H. Gonzalez, J. G. Solé, D. J. García, *Nano Res.* **2015**, *8*, DOI 10.1007/s12274-014-0549-1.

[26] K. Welsher, S. P. Sherlock, H. Dai, *Proc. Natl. Acad. Sci.* **2011**, *108*, 8943.

[27] J. T. Robinson, G. Hong, Y. Liang, B. Zhang, O. K. Yaghi, H. Dai, *J. Am. Chem. Soc.* **2012**, *134*, 10664.

[28] R. Bhavane, Z. Starosolski, I. Stupin, K. B. Ghaghada, A. Annapragada, *Sci. Rep.* **2018**, *8*, 14455.

[29] J. Huang, C. Xie, X. Zhang, Y. Jiang, J. Li, Q. Fan, K. Pu, *Angew. Chem. Int. Ed.* **2019**, *58*, 15120.

[30] Y. Lyu, J. Li, K. Pu, *Small Methods* **2019**, *3*, 1900553.

[31] Y. Jiang, P. K. Upputuri, C. Xie, Z. Zeng, A. Sharma, X. Zhen, J. Li, J. Huang, M. Pramanik, K. Pu, *Adv. Mater.* **2019**, *31*, 1808166.

[32] Q. Miao, K. Pu, *Adv. Mater.* **2018**, *30*, 1801778.

[33] A. Benayas, F. Ren, E. Carrasco, V. Marzal, B. del Rosal, B. A. Gonfa, Á. Juarranz, F.

Sanz-Rodríguez, D. Jaque, J. García-Solé, D. Ma, F. Vetrone, *Adv. Funct. Mater.* **2015**, *25*, 6650.

[34] Y. Imamura, S. Yamada, S. Tsuboi, Y. Nakane, Y. Tsukasaki, A. Komatsuzaki, T. Jin, *Molecules* **2016**, *21*, DOI 10.3390/molecules21081080.

[35] S. Jeong, Y. Jung, S. Bok, Y.-M. Ryu, S. Lee, Y.-E. Kim, J. Song, M. Kim, S.-Y. Kim, G.-O. Ahn, S. Kim, *Adv. Healthc. Mater.* **2018**, *7*, 1800695.

[36] S. I. Sadovnikov, A. I. Gusev, *J. Mater. Chem. A* **2017**, *5*, 17676.

[37] Y. Zhang, G. Hong, Y. Zhang, G. Chen, F. Li, H. Dai, Q. Wang, *ACS Nano* **2012**, *6*, 3695.

[38] G. Hong, J. T. Robinson, Y. Zhang, S. Diao, A. L. Antaris, Q. Wang, H. Dai, *Angew. Chem. Int. Ed.* **2012**, *51*, 9818.

[39] F. Hu, C. Li, Y. Zhang, M. Wang, D. Wu, Q. Wang, *Nano Res.* **2015**, *8*, 1637.

[40] H. D. A. Santos, E. C. Ximendes, M. del C. Iglesias-de la Cruz, I. Chaves-Coira, B. del Rosal, C. Jacinto, L. Monge, I. Rubia-Rodríguez, D. Ortega, S. Mateos, J. GarcíaSolé, D. Jaque, N. Fernández, *Adv. Funct. Mater.* **2018**, *28*, 1803924.

[41] C. Li, F. Li, Y. Zhang, W. Zhang, X. E. Zhang, Q. Wang, *ACS Nano* **2015**, *9*, 12255.

[42] Y. Zhang, Y. Zhang, G. Hong, W. He, K. Zhou, K. Yang, F. Li, G. Chen, Z. Liu, H. Dai, Q. Wang, *Biomaterials* **2013**, *34*, 3639.

[43] C. Li, Y. Zhang, M. Wang, Y. Zhang, G. Chen, L. Li, D. Wu, Q. Wang, *Biomaterials* **2014**, *35*, 393.

[44] J. Javidi, A. Haeri, F. Nowroozi, S. Dadashzadeh, *Pharm. Res.* **2019**, *36*, 46.

[45] L. Dong, G. Ji, Y. Liu, X. Xu, P. Lei, K. Du, S. Song, J. Feng, H. Zhang, *Nanoscale* **2018**, *10*, 825.

[46] X. Peng, J. Liu, B. Li, G. Guan, W. Zhang, X. Huang, Y. Chen, R. Zou, X. Lu, J. Hu, *Nanoscale* **2019**, *11*, 20324.

[47] T. Yang, Y. Tang, L. Liu, X. Lv, Q. Wang, H. Ke, Y. Deng, H. Yang, X. Yang, G. Liu,

Y. Zhao, H. Chen, *ACS Nano* **2017**, *11*, 1848.

[48] H. D. A. Santos, D. Ruiz, G. Lifante, C. Jacinto, B. H. Juarez, D. Jaque, *Nanoscale* **2017**, *9*, 2505.

[49] C. Lu, G. Chen, B. Yu, H. Cong, *Adv. Eng. Mater.* **2018**, *20*, 1700940.

[50] Y. Shen, J. Lifante, E. Ximendes, H. D. A. Santos, D. Ruiz, B. H. Juárez, I. Zabala Gutiérrez, V. Torres Vera, J. Rubio Retama, E. Martín Rodríguez, D. H. Ortgies, D. Jaque, A. Benayas, B. del Rosal, *Nanoscale* **2019**, DOI 10.1039/C9NR05733A.

[51] C. Wu, Y. Zhang, Z. Li, C. Li, Q. Wang, *Nanoscale* **2016**, *8*, 12531.

[52] G. Hong, J. C. Lee, A. Jha, S. Diao, K. H. Nakayama, L. Hou, T. C. Doyle, J. T. Robinson, A. L. Antaris, H. Dai, J. P. Cooke, N. F. Huang, *Circ. Cardiovasc. Imaging* **2014**, *7*, 517.

[53] B. Molavi, J. Chen, J. L. Mehta, *Am. J. Physiol. Circ. Physiol.* **2006**, *291*, H687.

[54] R. Hennig, K. Pollinger, J. Tessmar, A. Goepferich, *J. Drug Target.* **2015**, *23*, 681.

[55] T. Dvir, M. Bauer, A. Schroeder, J. H. Tsui, D. G. Anderson, R. Langer, R. Liao, D. S. Kohane, *Nano Lett.* **2011**, *11*, 4411.

[56] D. H. Ortgies, Á. L. García-Villalón, M. Granado, S. Amor, E. M. Rodríguez, H. D. A. Santos, J. Yao, J. Rubio-Retama, D. Jaque, *Nano Res.* **2019**, *12*, 749.

[57] V. Mirshafiee, M. Mahmoudi, K. Lou, J. Cheng, M. L. Kraft, *Chem. Commun.* **2013**, *49*, 2557.

[58] V. Mirshafiee, R. Kim, S. Park, M. Mahmoudi, M. L. Kraft, *Biomaterials* **2016**, *75*, 295.

[59] V. H. Nguyen, B. J. Lee, *Int. J. Nanomedicine* **2017**, *12*, 3137.

[60] J. Y. Oh, H. S. Kim, L. Palanikumar, E. M. Go, B. Jana, S. A. Park, H. Y. Kim, K. Kim, J. K. Seo, S. K. Kwak, C. Kim, S. Kang, J. H. Ryu, *Nat. Commun.* **2018**, *9*, 1.

[61] L. Pappas, G. Filippatos, *Rev. Española Cardiol. (English Ed.* **2011**, *64*, 735.

[62] L. Pavone, S. Albert, J. DiRocco, L. Gatto, G. Nieman, *Crit. Care* **2007**, *11*, R104.

[63] J. C. Grimm, F. Zhang, J. T. Magruder, T. C. Crawford, M. Mishra, K. M. Rangaramanujam, A. S. Shah, *J. Surg. Res.* **2017**, *210*, 78.

[64] E. K. Wolthuis, A. P. Vlaar, G. Choi, J. J. Roelofs, N. P. Juffermans, M. J. Schultz, *Crit. Care* **2009**, *13*, R1.

[65] J.-S. Jerng, Y.-C. Hsu, H.-D. Wu, H.-Z. Pan, H.-C. Wang, C.-T. Shun, C.-J. Yu, P.-C. Yang, *Thorax* **2007**, *62*, 527.

[66] Z. Xu, J. Alloush, E. Beck, N. Weisleder, *J. Vis. Exp.* **2014**, DOI 10.3791/51329.

[67] P. Chomzynski, *Anal. Biochem.* **1987**, *162*, 156.

[68] K. J. Livak, T. D. Schmittgen, *Methods* **2001**, *25*, 402.

[69] S. Zhu, S. Herraiz, J. Yue, M. Zhang, H. Wan, Q. Yang, Z. Ma, Y. Wang, J. He, A. L. Antaris, Y. Zhong, S. Diao, Y. Feng, Y. Zhou, K. Yu, G. Hong, Y. Liang, A. J. Hsueh, H. Dai, *Adv. Mater.* **2018**, *30*, 1705799.

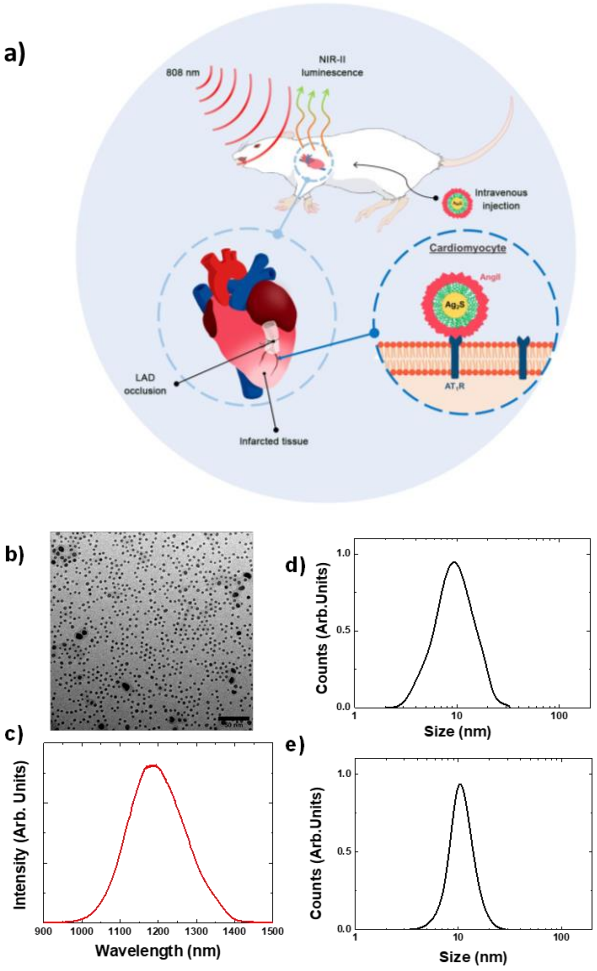

Figure 1. (a) Schematic representation of the experimental procedure followed in this work for *in vivo* imaging of acute infarct. **(b)** TEM image of Ag_2S NDs used in this work. Scale bar: 50 nm **(c)** Emission spectra obtained from a colloidal suspension of Ag_2S NDs as obtained under 790 nm optical excitation. **(d)** and **(e)** DLS graphs of AngII-functionalized and PEGylated Ag_2S NDs, respectively. In both cases a hydrodynamic radius close to 10 nm is obtained.

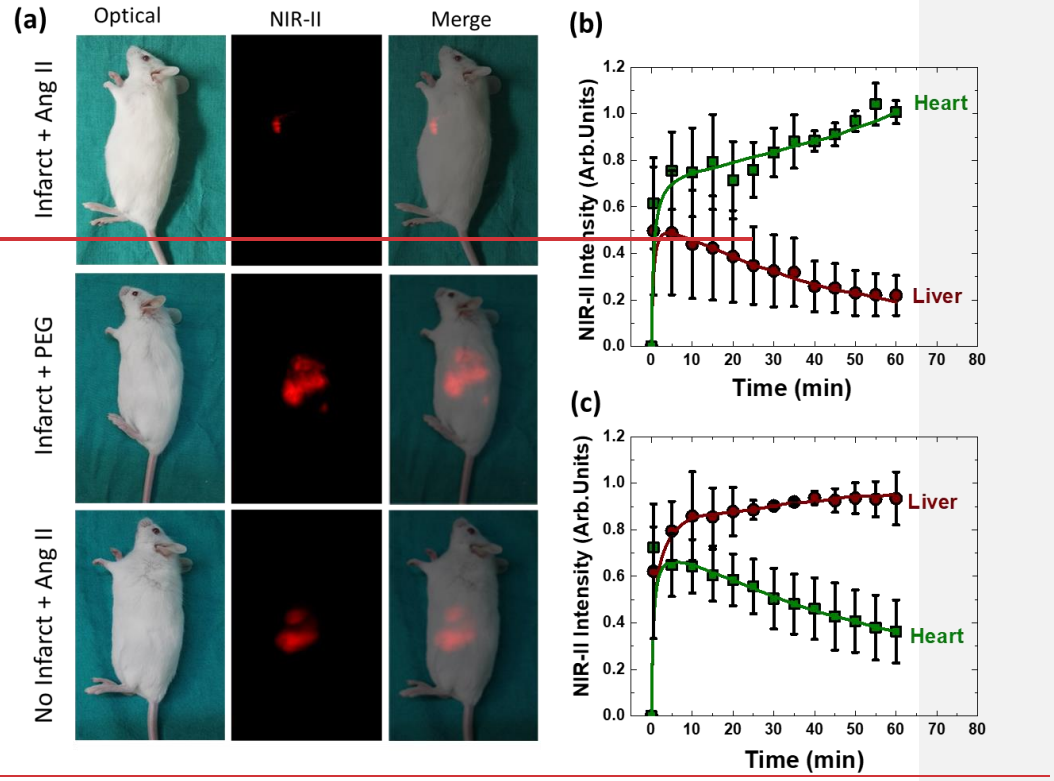

Figure 2. (a) Optical, NIR-II fluorescence (10 minutes after injection of Ag_2S NDs) and merged images of three representative mice corresponding to the three scenarios presented. Top row corresponds to a mouse subjected to an acute infarct followed by an intravenous injection of AngII-functionalized Ag_2S NDs. Middle row corresponds to a mouse subjected to an acute infarct followed by an intravenous injection of PEGylated Ag_2S NDs. Finally, the bottom row corresponds to a sham-operated mouse (without any infarct) subjected to an intravenous injection of AngII-functionalized Ag_2S NDs. **(b)** Time course of the average NIR-II luminescence intensity generated at the heart and liver of three mice subjected to an acute infarct and to an intravenous injection of AngII-functionalized Ag_2S NDs. **(c)** Time course of the average NIR-II luminescence intensity generated at the heart and liver of three mice subjected to an acute infarct and to an intravenous injection of PEGylated Ag_2S NDs. **(d)** Time course of the average NIR-II luminescence intensity generated at the heart and liver of a non-infarct mouse injected with AngII-functionalized Ag_2S NDs. Error bars have been estimated from the noise in the fluorescence images. In (b) ~~and (~~ ed) dots are experimental data and solid lines are a guide for the eyes.~~,~~ In (b) and (c) error bars correspond to the SEM.~~,~~ ~~and solid lines are a guide for the eyes.~~

Con formato: Fuente: 12 pto

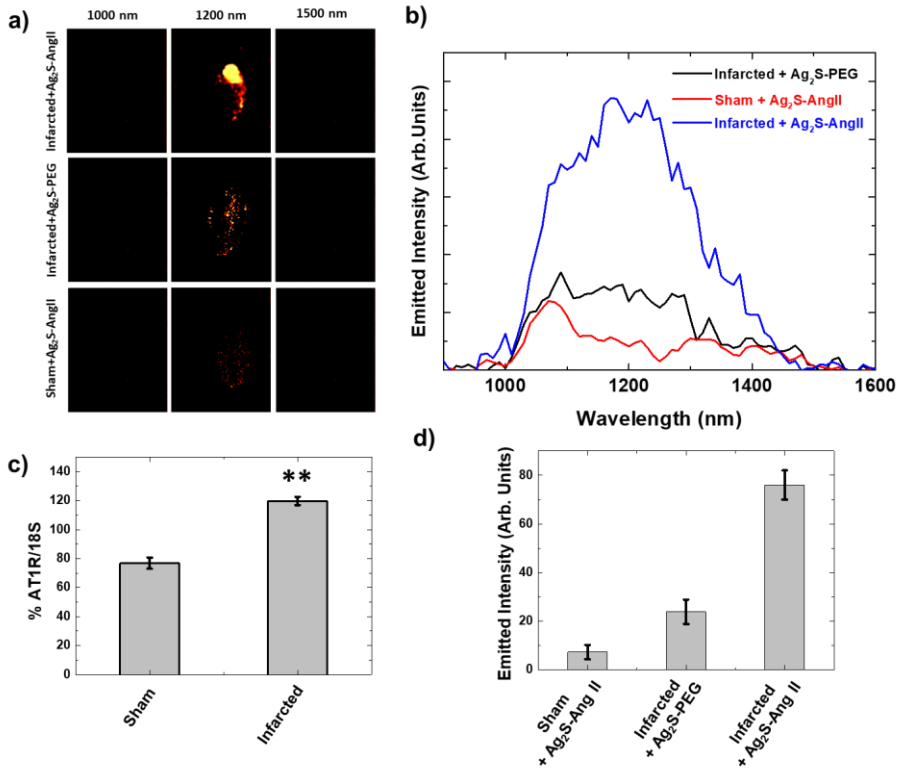

Figure 3. (a) *Ex vivo* fluorescence images at three different emission wavelengths (1000, 1200 and 1500 nm) as obtained for a heart subjected to an acute infarct and an intravenous injection of AngII-functionalized Ag_2S NDs, a heart subjected to an acute infarct and intravenous injection of PEGylated Ag_2S NDs, and a healthy heart from a sham-operated mouse subjected to an intravenous injection of AngII-functionalized Ag_2S NDs. The emission spectra corresponding to each case are shown in **(b)**. **(c)** mRNA levels of AT-1 in myocardial tissue from sham operated-mice and mice subjected to myocardial infarction. (**p<0.01 vs Sham). **(d)** Emitted intensity in the 1000-1600 nm range by a healthy heart (Sham + Ag_2S-AngII), an infarcted heart after intravenous injection with PEGylated Ag_2S NDs (Infarcted + Ag_2S-PEG), and an infarcted heart after i.v. injection of AngII-functionalized Ag_2S NDs.

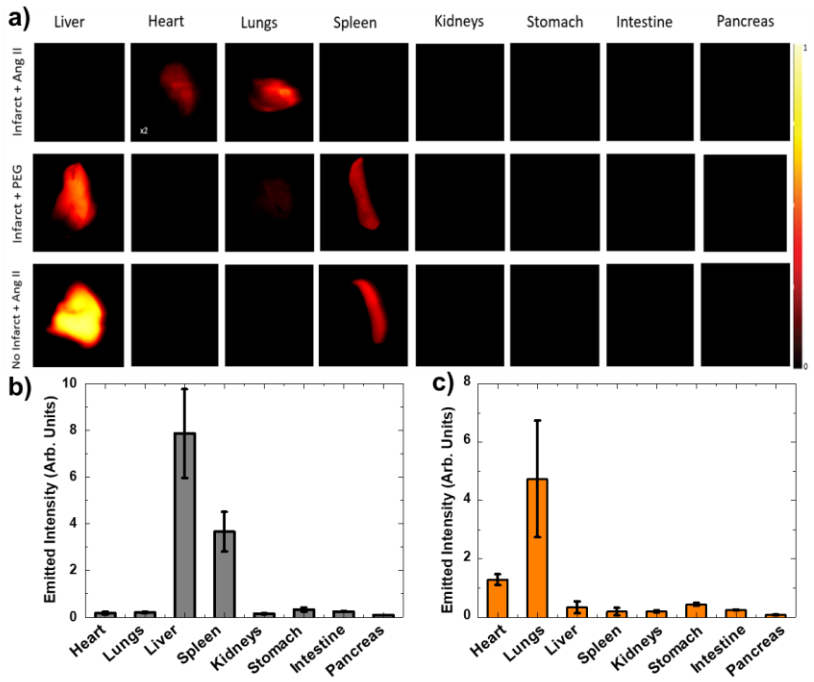

Figure 4. (a) *Ex vivo* NIR-II fluorescence images of the dissected organs corresponding to an infarcted mouse after intravenous injection of AngII-functionalized Ag_2S NDs, to a mouse subjected to an acute infarct and subsequent intravenous injection with PEGylated Ag_2S NDs, and a sham-operated mouse (no infarct) injected withAg_2S-AngII NDs. Intensity histograms of the luminescence generated by the Ag_2S NDs accumulated in the different organs as obtained for three mice subjected to an acute infarct and to a subsequent intravenous injection with PEGylated Ag_2S NDs (**(b)**) and with AngII-functionalized Ag_2S NDs (**(c)**).

Table 1. *In vivo* NIR fluorescence imaging of myocardial infarction with luminescent nanoparticles. Previous works were able to visualize damage 2 days post injection for permanent ligation and 1 day after injection in a reversible ligation / reperfusion case, employing NIR-I imaging close to the visible. In contrast, this work allows direct near real-time imaging of acute infarction 30 minutes post reperfusion and less than 10 minutes after injection of Ag_2S NDs.

Nanoparticle system	λexc [nm]	λem [nm]	Functionalization	Type of myocardial infarct	Time after injection for heart imaging	Ref.
Clio-Cy5.5	672	680-720	Dextran/Cy 5.5	Permanent ligation	2 days	[13]
CLIO-VT750	750	780	Dextran protease substrates	Permanent ligation / reperfusion	1 day	[14]
Prosense680	680	700				
Ag_2S-AngII	808	1200	PEG-AngII	Reperfusion	Minutes	This work

Angiotensine II-functionalized Ag_2S nanodots enable rapid *in vivo* NIR-II imaging of damage to the myocardium after a heart attack in mice. Less than 10 min after intravenous injection specific images are obtained and can be distinguished from control cases (non-targeted nanoparticles and healthy mice).

Keyword NIR-II bioimaging, Ag_2 nanodots, infarcted heart, cardiovascular imaging.

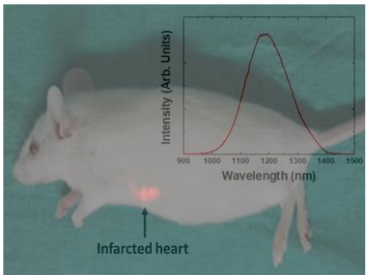

Sergio Mateos, José Lifante, Chunyan Li, Erving C. Ximendes, Tamara Muñoz-Ortiz, Jingke Yao, María de la Fuente, Ángel Luis García Villalón, Miriam Granado, Irene Zabala Gutiérrez, Jorge Rubio Retama, Daniel Jaque, Dirk H. Ortgies, and Nuria Fernández

Instantaneous in vivo imaging of acute myocardial infarct by NIR-II luminescent nanodots

Supporting Information

Instantaneous in vivo imaging of acute myocardial infarct by NIR-II luminescent nanodots

Sergio Mateos,[+] José Lifante,[+] Chunyan Li, Erving C. Ximendes, Tamara Muñoz-Ortiz, Jingke Yao, María de la Fuente, Ángel Luis García Villalón, Miriam Granado, Irene Zabala Gutiérrez, Jorge Rubio Retama, Daniel Jaque, Dirk H. Ortgies,* and Nuria Fernández*

S1. Additional TEM micrograph of PEGylated Ag_2S NDs

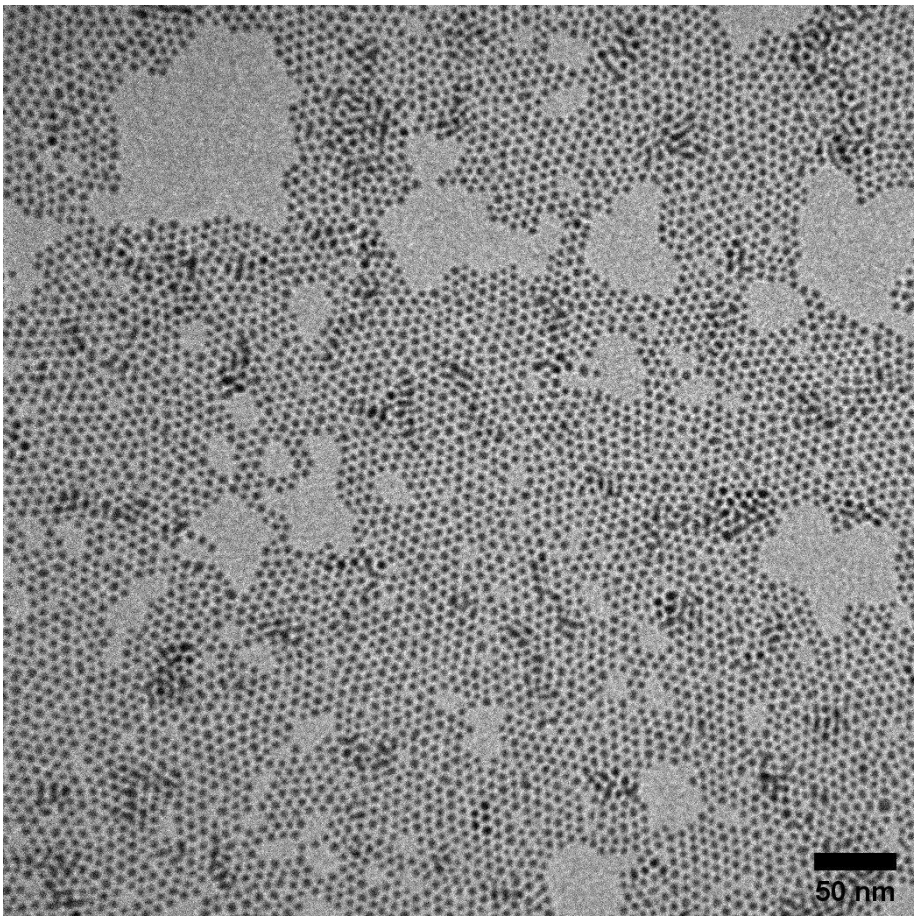

Figure S1. TEM Micrograph of PEGylated Ag_2S NDs

S2. FTIR characterization of Ag_2S NDs

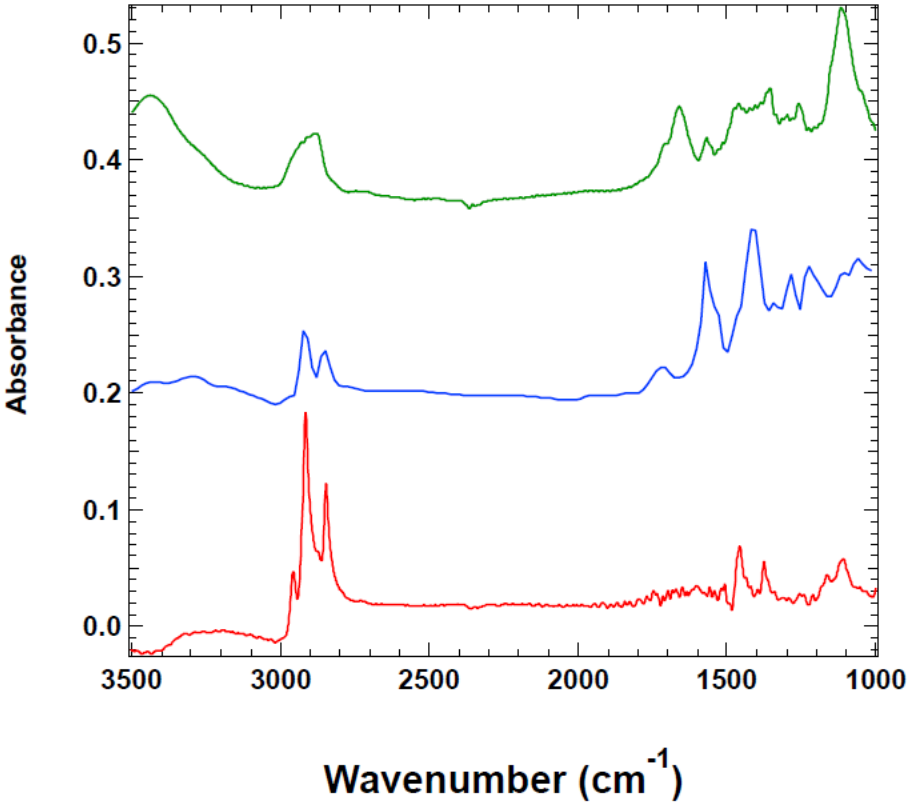

Figure S2. FTIR spectra of Ag_2S NDs with different surface functionalities; dodecanethiol-capped Ag_2S NPs in red, 11-mercaptoundecylcarboxylic acid capped Ag_2S NPs in blue and PEG (MW=2500 g/mol) functionalized Ag_2S NDs in green. All the spectra were acquired in a Nicolet IR200 FTIR spectrometer.

S3. Merged NIR-II and optical images over the duration of all three cases

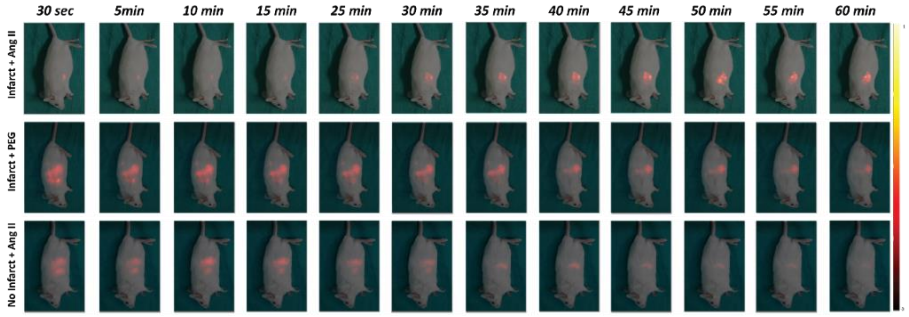

Figure S3. Fluorescence images obtained at different times after intravenous injection of Ag_2S NDs. Images corresponds to three different mice each of them being representative of the three cases studied in this work: Top row) mouse subjected to an infarct followed by an intravenous injection of AngII-functionalized Ag_2S NDs (Infarct+AngII). Middle row) mouse subjected to an infarct followed by an intravenous injection of PEGylated Ag_2S NDs. Bottom row) a sham-operated mouse with an intravenous injection of AngII-functionalized Ag_2S NDs (No infarct+AngII). The times of the column show the time after injection when the NIR-II imaging was performed and the scale on the right reflects the intensity of the Ag_2S NDs luminescence.

S4. Detailed analysis of individual time courses for AngII-functionalized NDs

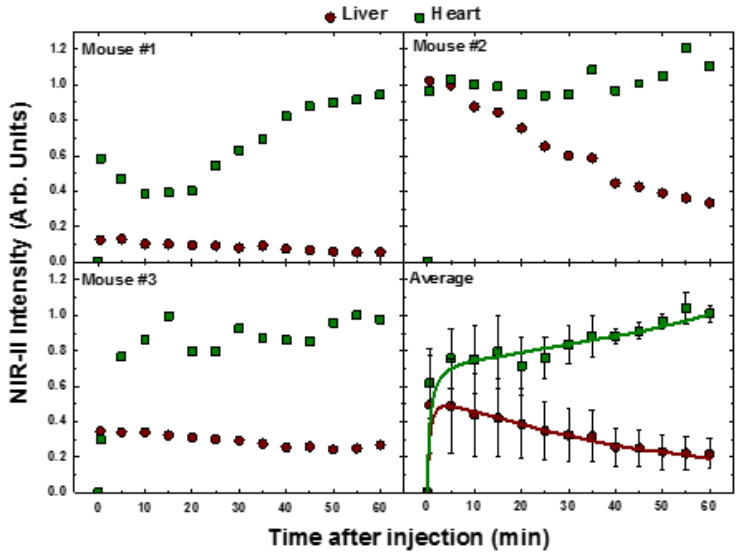

Figure S4. Time course profiles obtained for the three mice corresponding to the "Infarct+AngII" case (mice subjected to an infarct followed by an intravenous injection of AngII-functionalized Ag_2S NDs). The average of the results obtained from the three different mice are also included. The error bars in the averaged time courses were calculated as the standard deviation of the mean (SEM). Symbols are experimental and averaged data and solid lines are guides for the eyes.

S5. Detailed analysis of individual time courses for PEGylated NDs

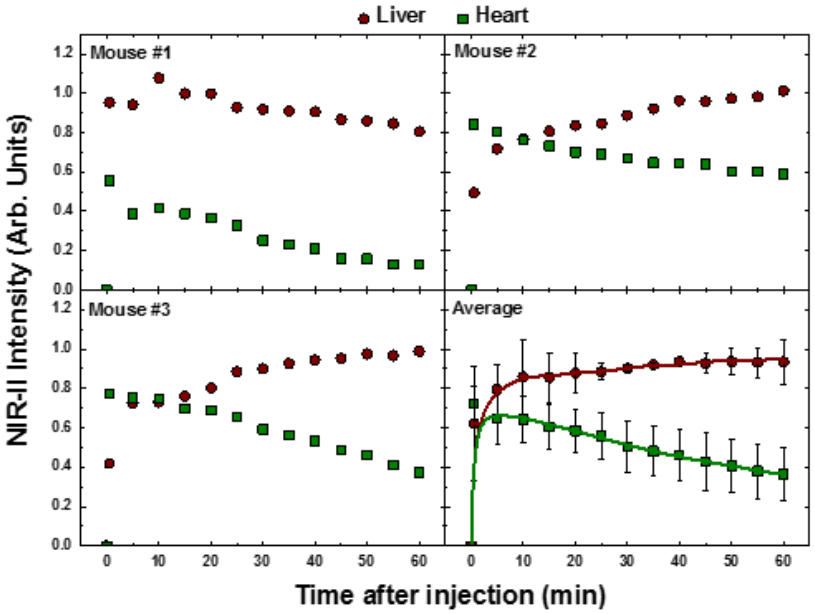

Figure S5. Time course profiles obtained for the three mice corresponding to the "Infarct+PEG" case (mice subjected to an infarct followed by an intravenous injection of PEGylated Ag_2S NDs). The average of the results obtained from the three different mice is also included. The error bars in the averaged time course are calculated as the SEM. Symbols are experimental and averaged data and solid lines are guides for the eyes.

S6. Circulation times of Ag_2S NDs

The characteristic circulation time was estimated by means of an experiment in which l00 μl of a solution of 1.5 mg mL^{-1} AngII-functionalized Ag_2S NDs were intravenously injected into an ischemic and a sham-operated mouse, and the luminescence intensity of the femoral artery was observed for 20 minutes. The NIR-II fluorescence generated by the AngII-functionalized Ag_2S NDs circulating in the bloodstream of the different mice followed similar patterns. A stage of monotonous increment was defined from the initial moment up to 147 seconds after the intravenous injection. This stage, in turn, was followed by another one characterized by a monotonous decrease of intensity that deviated from a single-exponential decay. The decay times, as obtained with the area under the decay curves, of the ischemic and the sham mouse were 490 and 507 s, respectively. If one defines the extrapolated circulation time as the maximum time in which one can still detect the luminescence coming from the luminescent probes (for instance, by setting a threshold of 5% for the normalized intensity), the data of Figure S6c provide 20 minutes and 30 s for the sham mouse and 21 minutes and 30 s for the ischemic one.

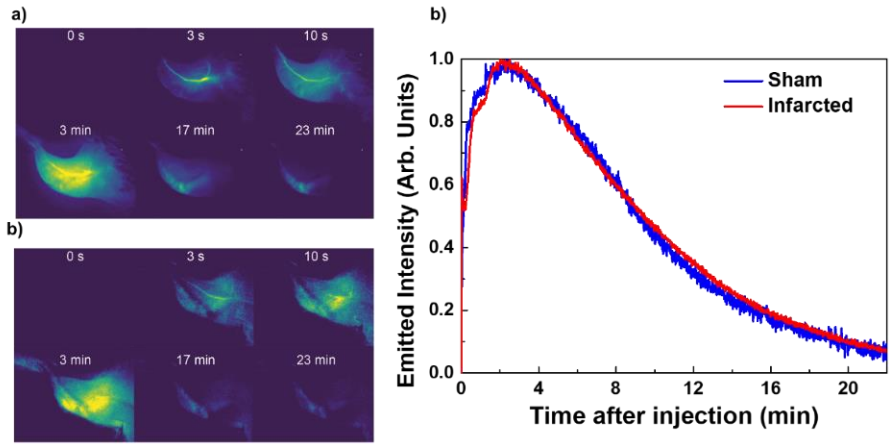

Figure S6. Fluorescence images obtained after intravenous injection of PEGylated Ag_2S NDs into **(a)** an ischemic CD1 mouse and **(b)** a sham mouse at different timepoints. **(c)** Time-evolution of the emitted intensity at the femoral artery of the ischemic (red) and SHAM (black) mice through the analysis of luminescence images.

S7. *Ex vivo* spectra of infarcted hearts

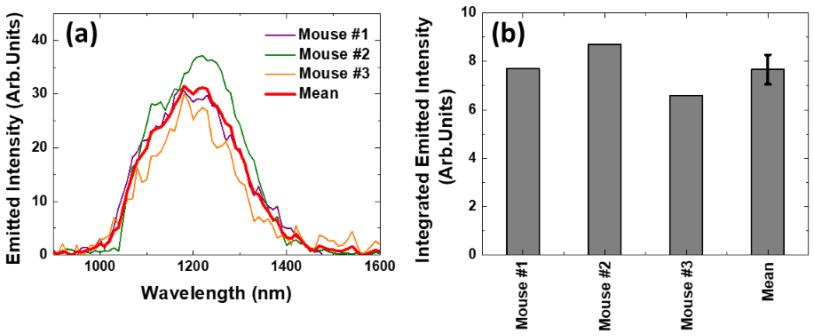

Figure S7. (a) Emission spectra obtained from the hearts corresponding to the three mice subjected to an infarct and to a subsequent intravenous injection of AngII-functionalized Ag_2S NDs. The averaged spectrum is also included. **(b)** Integrated intensities generated by the heart of the three mice subjected to an infarct and a subsequent intravenous injection of AngII-functionalized Ag_2S NDs as obtained from **(a)**. The integrated emissions of the three mice have been used to calculate the error as their SEM.

S8. Triphenyl Tetrazolium Chloride (TTC) staining for infarction assessment

The myocardial infarct size was determined by a TTC staining of the explanted hearts. The hearts were kept frozen at -80 ºC prior to the staining. The heart was cut into slices of 1 mm and incubated with TTC 1% during 20 minutes at 37 ºC, after that the slices were placed in phosphate buffered saline (PBS) overnight, which increased the contrast between the infarct area and the healthy area, thus obtaining a better visualization of the tissue. TTC precipitates with red colour if the tissue is non-affected by the infarct because mitochondria dehydrogenases are active and can perform the reaction with the dye, while dead tissue remains pale. (Redfors B, Shao Y, Omerovic E. Myocardial infarct size and area at risk assessment in mice. Experimental and clinical cardiology 2012;17(4):268.)

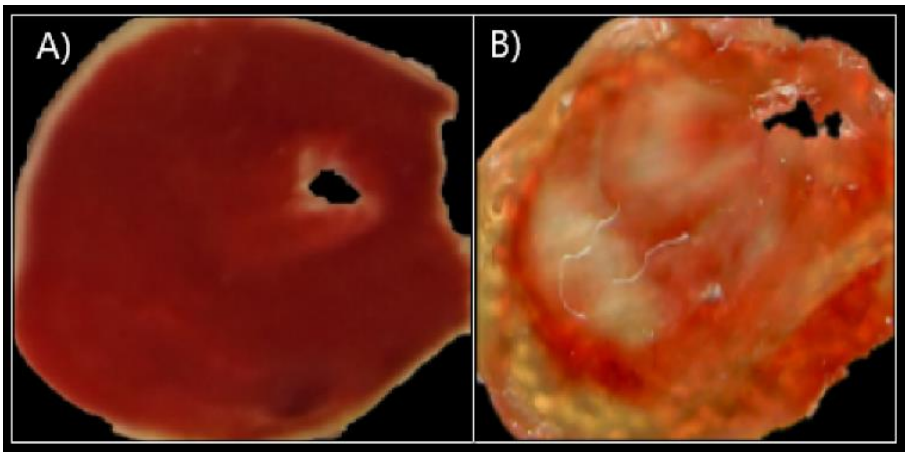

Figure S8. (**a**) A control heart (sham operation) that shows only healthy tissue and no damaged tissues after TTC staining (**b**) In the cut obtained from an infarcted heart the damaged tissues are identified after staining pale areas, while healthy tissues stay red.